High Thermoelectric Figure of Merit of Full-Heusler Ba₂AuX (X = As, Sb, and Bi)

Jinlong Ma, Arun S. Nissimagoudar, Shudong Wang, and Wu Li*

Herein, an unprecedentedly high thermoelectric figure of merit (ZT) in full-Heusler compounds of Ba_2AuX (X = As, Sb, and Bi) is predicted by performing first-principles calculations combined with parameter-free Boltzmann transport equations. It is found that the ZT can reach up to 5 and 3 at 800 K in n- and p-type systems, respectively, and can be as high as 1.7 and 1.0 at room temperature. The high ZT is attributed to the high power factor coupled with low thermal conductivity. The spin–orbit coupling (SOC) is necessarily considered because the exclusion of SOC significantly overestimates the electron mobility but underestimates the hole mobility of Ba_2AuBi. The Lorenz number is found to exhibit an expected monotonical increase with carrier concentration, in contrast to the reported literature results.

Developing high-performance thermoelectric materials is at the core of thermoelectrics, which is the simplest technology applicable to direct green heat-to-electricity energy conversion. To achieve a high conversion efficiency, gauged by the figure of merit $ZT = \frac{S^2 \sigma T}{\kappa_e + \kappa_{ph}}$, the materials should simultaneously possess a high electrical conductivity (σ) and Seebeck coefficient (S) but a low thermal conductivity containing contribution from electrons (κ_e) and phonons (κ_{ph}). The $\{S, \sigma, \kappa_e\}$ are inversely interdependent such as the increase in σ followed by the decrease in S and increase in κ_e; thus, optimizing ZT is a delicate trade-off between these electrical properties.[1] In contrast, κ_{ph} is relatively decoupled. Therefore, one of the mainstream strategies for high ZT is searching materials with an intrinsically low κ_{ph}.[2–4]

From the computational point of view, the solutions of Boltzmann transport equations (BTE) with the phonon–phonon and electron–phonon scattering based on density functional theory

Dr. J. Ma
School of Energy and Power Engineering
Huazhong University of Science and Technology
Wuhan 430074, China

Dr. A. S. Nissimagoudar, Dr. W. Li
Institute for Advanced Study
Shenzhen University
Shenzhen 518060, China
E-mail: wu.li@szu.edu.cn

Dr. S. Wang
School of Physical Science and Technology
Inner Mongolia University
Hohhot 010021, China

The ORCID identification number(s) for the author(s) of this article can be found under https://doi.org/10.1002/pssr.202000084.

(DFT) have enabled accurate parameter-free calculations of κ_{ph}[5–10] and $\{S, \sigma, \kappa_e\}$.[11–21] Recent calculations revealed that a series of full-Heusler compounds possess ultra-low κ_{ph} and dispersive band structures,[22] which insinuate good promise for the thermoelectric applications. Recently, a high ZT has been demonstrated in Ba_2AuBi by first-principles calculations.[23] Nonetheless, the spin–orbit coupling (SOC) was not considered, which, however, affects the band structure of Ba_2AuBi significantly[23] and thus the electrical transport properties would be altered.[16,18] Moreover, the BTE was solved under relaxation time approximation (RTA), which generally underestimates the electrical mobility in polar materials due to the strong coupling of the electrons with longitudinal optical (LO) phonons, i.e., long-range Fröhlich interactions.[15–17] Therefore, we carried out first-principles calculations for the thermoelectric properties of Ba_2AuBi as well as Ba_2AuSb and Ba_2AuAs considering the SOC and exact solutions of BTE[11,15,16] and found that all the three Ba_2AuX have high ZT, due to their low thermal conductivities and promising power factors (PF).

The DFT calculations were carried out using Quantum ESPRESSO package,[24] with the full-relativistic norm-conserving pseudopotentials generated by the latest multiprojector ONCVPSP code[25] and the inputs of SG15 pseudopotentials.[26] Generalized gradient approximation in the form of Perdew–Burke–Ernzerhof (PBE)[27] was used for the exchange-correlation functional. Ba_2AuX has a face-centered cubic crystal structure with $Fm\bar{3}m$ symmetry (Figure S1, Supporting Information), and the relaxed lattice constants are 8.01, 8.28, and 8.38 Å for Ba_2AuAs, Ba_2AuSb, and Ba_2AuBi, respectively (Figure S2, Supporting Information). The initial electron energies, phonon frequencies, and electron–phonon coupling interactions were conducted on $8 \times 8 \times 8$ **k** and $4 \times 4 \times 4$ **q** grids. For $\{S, \sigma, \kappa_e\}$ calculations (Section 1, Supporting Information), these intermediate quantities were interpolated to $48 \times 48 \times 48$ **k** and $48 \times 48 \times 48$ **q** points by Wannier function interpolation used with EPW package.[28] As has been verified that the SOC almost has no effect on κ_{ph},[22] the SOC was not included in the calculation of interatomic force constants (IFCs). The second-order IFCs were calculated on $4 \times 4 \times 4$ **q** grids, whereas the third-order IFCs were calculated with the $3 \times 3 \times 3$ supercell constructed from the primitive unit cell and a distance truncation of 0.6 nm was used. Then the ShengBTE package[5] was used to calculate κ_{ph} with $32 \times 32 \times 32$ **q** samplings.

In our calculations, only the phonon-limited intrinsic properties are calculated, which neglects a few effects such as impurity

ADVANCED
SCIENCE NEWS
www.advancedsciencenews.com

physica
pss status solidi rrl
www.pss-rapid.com

scattering, phonon drag, and so forth. These factors would alter the thermoelectric properties. Nevertheless, as recently illustrated in SnSe,[29] the intrinsic calculations especially for electrical transport can give reasonable values compared with the experiments. In semiconductors with narrow bandgaps, the electron and hole transport coexist due to the thermal excitation. The bipolar transport would decrease the Seebeck coefficient due to the opposite contribution from electron and hole and increase the thermal conductivity due to the presence of nonzero Peltier heat carried by electron and hole currents.[30,31] As a consequence, the ZT is reduced. Increasing the bandgap by some strategies such as alloying can prevent the degradation caused by the bipolar effect.[30,32] A bandgap on the order of 10 $(k_\mathrm{B}T)$ is typically enough to effectively minimize the contribution of minority carriers.[31] As for Ba_2AuX (X = As, Sb, and Bi), the DFT calculated bandgaps are 0.50, 0.59 and 0.30 eV respectively, which are underestimated due to the drawback of PBE approximation. We have confirmed that the bandgaps with GW correction using YAMBO package[33] are opened up to 1.20, 0.79, and 0.76 eV, respectively, close to previous calculations with HSE hybrid functional without SOC.[22] In this work, we only focus on the properties below 800 K, corresponding to a thermalization energy of $10(k_\mathrm{B}T)$ at $\approx$0.69 eV. Therefore, the bipolar effect is neglected and the electron and hole transports are calculated separately.

Figure 1a shows the calculated intrinsic mobilities of Ba_2AuX at different temperatures. We have checked that the RTA solution of BTE indeed underestimates the mobility, about 13–17%, 12–14%, and 7–9% for Ba_2AuAs, Ba_2AuSb, and Ba_2AuBi in the temperature range of 300–800 K, respectively. The smallest underestimation in Ba_2AuBi suggests the weakest Fröhlich effect, which is proportional to the frequency of LO phonons and inversely proportional to dielectric permittivity.[34] Ba_2AuBi has the largest dielectric permittivity, about 36.1, whereas it is 24.6 for Ba_2AuSb and 28.4 for Ba_2AuAs. Meanwhile, the phonon frequency of Ba_2AuBi is also the lowest due to its heavy atomic mass (Figure S4, Supporting Information). At room temperature, the electron mobilities of Ba_2AuAs, Ba_2AuSb, and Ba_2AuBi are 516, 298 and 504 $cm^2\,V^{-1}\,s^{-1}$,

respectively, whereas they are 115, 141, and 285 $cm^2\,V^{-1}\,s^{-1}$ for holes. The electron mobility of Ba_2AuSb is the smallest, in line with its highest scattering rates, as shown in Figure 1b. Previous studies have clarified that the mobility is significantly affected by the band structure characterized by the effective mass around band edges and the energy difference between different valleys.[16,18,35] As shown in Figure 1c, for Ba_2AuSb, the electron-effective mass is the heaviest and the energy difference between conduction valleys is the smallest, which results in the low velocity, high scattering phase space, and earlier appearance of intervalley scattering. Analogously, the hole mobility of Ba_2AuBi is the highest due to its small effective mass and large valley gaps.

The mobilities of Ba_2AuBi excluding SOC are also given, which are overestimated for electrons and underestimated for holes. This is also related to the change of band structure, as discussed previously; for instance, the hole effective mass of Ba_2AuBi around the valence band edge is overestimated by the exclusion of SOC (Figure S3, Supporting Information). As temperature increases, the overestimation for electrons increases from 20% at 300 K to 80% at 800 K, whereas the underestimation for holes decreases from 50% at 300 K to 15% at 800 K. This can be understood from the comparison of scattering rates, as shown in Figure 1b. In the 300–800 K temperature range, more than 95% mobilities are contributed by electrons or holes with energy smaller than 0.3 eV. The exclusion of SOC weakens the scattering for electrons in the whole energy range, whereas for holes the scattering above 0.2 eV is also weakened but the scattering below 0.2 eV is enhanced. As temperature increases, the contribution from the charge carrier with a high energy increases; correspondingly, the high-energy contribution amplifies the overestimation in electrons but compensates the underestimation from low-energy holes. Because the conduction and valence band edges are mainly formed by the Ba and X atoms respectively,[22] the SOC also affects the band structures of Ba_2AuSb and Ba_2AuAs especially for conduction bands (Figure S3, Supporting Information), and thus the SOC is also included.

In experiments, the total thermal conductivity is measured and is hard to be separated into κ_e and κ_ph. The Wiedemann–
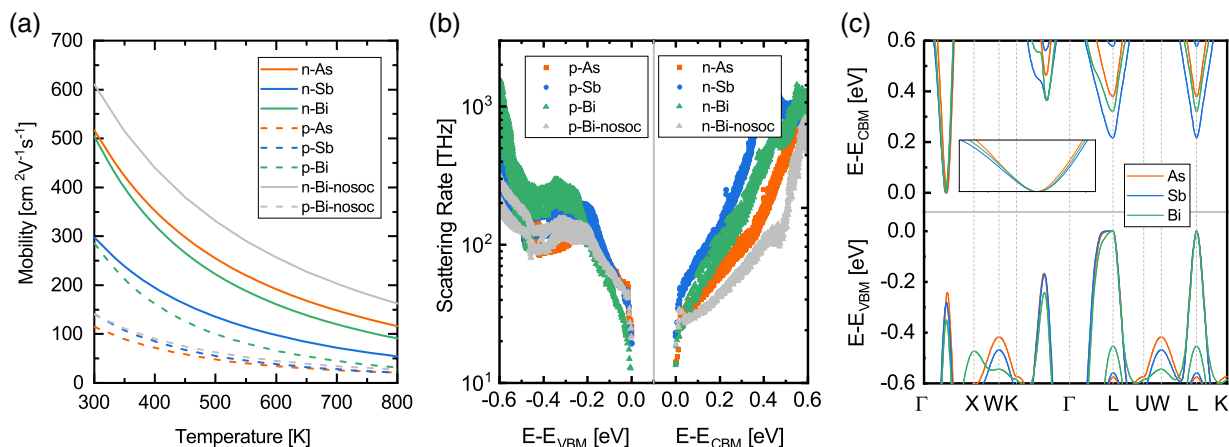
Figure 1. a) Intrinsic electron and hole mobilities of Ba_2AuX (X = As, Sb, and Bi) and b) the corresponding electron and hole scattering rates at room temperature. c) Band structures of Ba_2AuX with the band edges moving to zero energy, in which the inset shows the comparison of the zoomed-in conduction band edges.
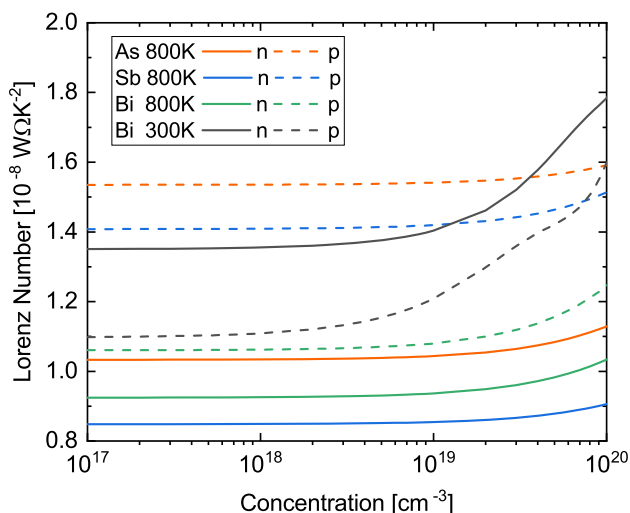
Figure 2. Lorenz number of Ba$_2$AuX (X = As, Sb, and Bi) as a function of carrier concentration at different temperatures.

Franz law ($\kappa_e = L\sigma T$) originating from metal systems is widely adopted and thus the Lorenz number (L) is an important parameter. As is known, the L of semiconductors has a more complicated behavior than that of metals and deviates from the Sommerfeld value of 2.24×10^{-8} WΩK^{-2}. Nonetheless, the L should be at a close order of magnitude, as analyzed from the nondegenerate single parabolic band model,[36] and has been illustrated in Si,[13,36] SnTe,[37] and SnSe.[29] However, Park et al.[23] displayed an implausibly deviated L for Ba$_2$AuBi at 800 K. Therefore, we calculated the L of n- and p-type Ba$_2$AuBi at different temperatures, as shown in **Figure 2**. The concentration dependence of L is similar to Si, SnSe, and n-type Ba$_2$AuBi at 300 and 500 K in a previous study[23] but different from 800 K therein. As temperature decreases, the L is slightly increased but still keeps an increasing trend as concentration increases. The more robust L of this work perhaps comes from the better-converged scattering rates as compared with a previous study.[23] The L of Ba$_2$AuSb and Ba$_2$AuAs exhibits a similar concentration dependence, as shown in Figure 2.

Figure 3 shows the calculated ZT of Ba$_2$AuX at carrier concentrations of 10^{17}–10^{20} cm^{-3} and several temperatures in 300–800 K. It can be seen that not only Ba$_2$AuBi but also Ba$_2$AuSb and Ba$_2$AuAs possess a high ZT in the whole temperature range. At 800 K, the n-type ZT can reach up to 4.8 in Ba$_2$AuBi at a concentration of 1×10^{19} cm^{-3}, whereas the p-type ZT is as high as 2.9 in Ba$_2$AuSb at a concentration of 4×10^{19} cm^{-3}. At room temperature, the highest ZT of n-type Ba$_2$AiBi is 1.7 at 7×10^{18} cm^{-3}, whereas in the p-type counterpart it is about 1.0 at 9×10^{18} cm^{-3}. The highest room-temperature ZT are 1.2 and 1.0 for n- and p-type Ba$_2$AuSb and 1.1 and 0.7 for n- and p-type Ba$_2$AuAs, respectively. The predicted room-temperature ZT values of Ba$_2$AuX are larger than many materials reported before,[1,2] including the hot thermoelectric material of SnSe, not only compared with its experimental results[38–40] but also its first-principles calculated values.[29] This indicates that Ba$_2$AuX would have promising thermoelectric performance in a wide temperature range for both n- and p-type systems. The carrier concentration is calculated based on rigid band approximation (RBA), and thus the change of band structure caused by the realistic doping and temperature is not considered. In previous studies of single-crystal SnSe with a carrier concentration below 10^{20} cm^{-3}, the RBA can produce a reasonable agreement with experiments in Seebeck coefficients,[41] electrical mobility,[17] electrical conductivity, and thermoelectric ZT.[29] Therefore, the RBA is used in the calculations and the carrier concentration dependence still plays a guiding role to a certain extent.

The calculated room-temperatures κ_{ph} are 0.92, 0.56, and 0.47 W m^{-1} K^{-1} for Ba$_2$AuX (X = As, Sb, and Bi), respectively, which are in good agreement with previous results.[22] This conforms the common situation that the identical lattice system with heavier atoms always possesses a lower κ_{ph}. The exclusion of nonanalytical correction leads to 2% underestimation of κ_{ph} (Figure S5, Supporting Information). The low κ_{ph} indicates strong phonon–phonon scattering and small mean-free paths (MFPs), especially at elevated temperatures (Figure S6, Supporting Information). The doping can effectively decrease κ_{ph} when the defect-scattering induced by dopant is comparable with phonon–phonon scattering. Thus, the reduction is significant in high-κ_{ph} materials such as Si ($\approx$50% at a concentration
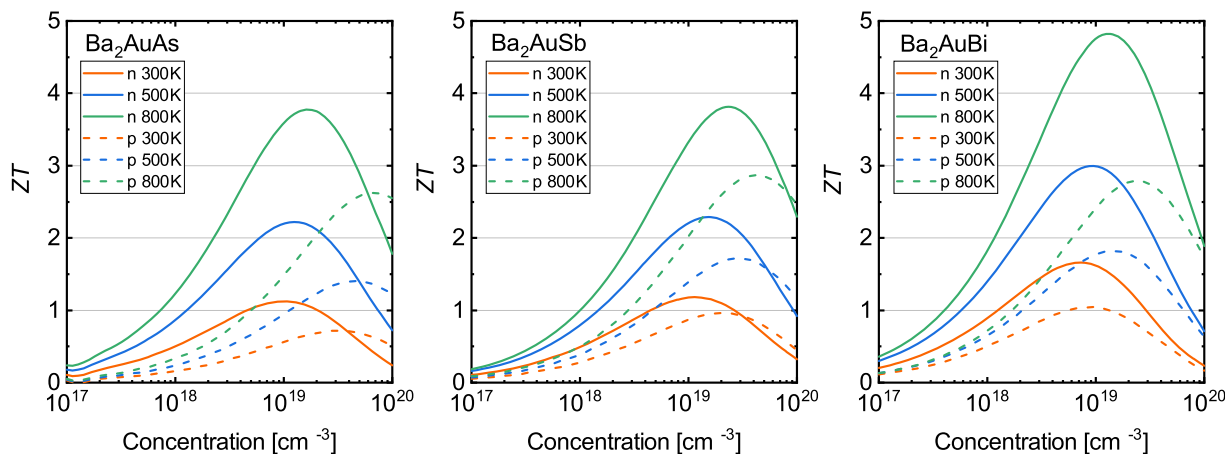
Figure 3. Calculated thermoelectric ZT of n- and p-type Ba$_2$AuX (X = As, Sb, and Bi) as a function of carrier concentrations.

of 10^{20} cm^{-3}),[42] whereas it is weak in low-κ_{ph} systems such as SnSe ($\approx$10% at a concentration of 10^{20} cm^{-3}), which has intrinsic values at about 0.7–2.0 W m^{-1} K^{-1}.[29] The phonon–phonon scattering of Ba$_2$AuX is comparable with that of SnSe.[29] Therefore, the κ_{ph} of single-crystal Ba$_2$AuX would not be significantly decreased by doping. Also, because of the small MFPs, the effect of grain scattering can be eliminated once the grain size is about few hundreds nanometers. Moreover, as concentration increases, the contribution of κ_e becomes comparable with κ_{ph}. For instance, at 800 K the κ_{ph} of Ba$_2$AuX (X = As, Sb, and Bi) decreases to 0.35, 0.21, and 0.18 W m^{-1} K^{-1}, respectively, whereas κ_e are 0.30, 0.12, and 0.11 W m^{-1} K^{-1} at an optimal concentration. As a consequence, the enhancement of ZT caused by the decrease in κ_{ph} is not significant. In addition, doping also affects the electrical transport properties. However, considering that S is less affected because it is mainly determined by the band structure,[17,41] and the simultaneous decrease in σ and κ_e are canceled to some extent, the calculated ZT could be close to the measured value, as has been recently illustrated in SnSe.[29] Under the optimal concentration at 800 K, the PFs ($= S^2 \sigma$) are 30, 16, and 17 μW cm^{-1} K^2 for n-type Ba$_2$AuAs, Ba$_2$AuSb, and Ba$_2$AuBi, respectively. These PF values are relatively high in thermoelectrics, for instance, the highest PF of the high-temperature phase SnSe is only about 10–15 μW cm^{-1} K^2 at 773 K.[38–40] Although the PF of Ba$_2$AuBi is only about half of that in Ba$_2$AuAs, the low total thermal conductivity leads to the high ZT. The high PF and low thermal conductivity of Ba$_2$AuX are the primary sources of high thermoelectric properties, which obeys the classic phonon-glass electron-crystal thermoelectric paradigms.

In summary, we calculated the electrical and thermal transport properties as well as the thermoelectric figure of merit of Ba$_2$AuX (X = As, Sb, and Bi) based on first-principles calculations and BTE. The SOC was considered and the BTE was accurately solved in an iterative framework beyond RTA. It is found that the RTA underestimates the mobility, and the inclusion of SOC is important due to its alteration on band structure. The three full-Heuslers are predicted to possess an unprecedentedly high ZT in both n- and p-type systems, as high as 5 and 3 at 800 K, respectively. Moreover, the room-temperature ZT is also promising with values larger than 1, which is higher than most of the thermoelectric materials found before, suggesting good potential for wide-temperature thermoelectric applications.

Supporting Information

Supporting Information is available from the Wiley Online Library or from the author.

Acknowledgements

Conflict of Interest

The authors declare no conflict of interest.

Keywords

[1] T. Zhu, Y. Liu, C. Fu, J. P. Heremans, J. G. Snyder, X. Zhao, *Adv. Mater.* **2017**, *29*, 1605884.
[2] G. J. Snyder, E. S. Toberer, *Nat. Mater.* **2008**, *7*, 105.
[3] X. Shi, L. Chen, C. Uher, *Int. Mater. Rev.* **2016**, *61*, 379.
[4] H. Kleinke, *Chem. Mater.* **2010**, *22*, 604.
[5] W. Li, J. Carrete, N. A. Katcho, N. Mingo, *Comput. Phys. Commun.* **2014**, *185*, 1747.
[6] T. Tadano, Y. Gohda, S. Tsuneyuki, *J. Phys.: Condens. Matter.* **2014**, *26*, 225402.
[7] A. Togo, L. Chaput, I. Tanaka, *Phys. Rev. B* **2015**, *91*, 094306.
[8] J. Ma, W. Li, X. Luo, *Phys. Rev. B* **2014**, *90*, 035203.
[9] D. A. Broido, M. Malorny, G. Birner, N. Mingo, D. A. Stewart, *Appl. Phys. Lett.* **2007**, *91*, 231922.
[10] A. Ward, D. Broido, D. Stewart, G. Deinzer, *Phys. Rev. B* **2009**, *80*, 125203.
[11] W. Li, *Phys. Rev. B* **2015**, *92*, 075405.
[12] J. Zhou, B. Liao, B. Qiu, S. Huberman, K. Esfarjani, M. S. Dresselhaus, G. Chen, *Proc. Natl. Acad. Sci. USA* **2015**, *112*, 14777.
[13] M. Fiorentini, N. Bonini, *Phys. Rev. B* **2016**, *94*, 085204.
[14] J. J. Zhou, M. Bernardi, *Phys. Rev. B* **2016**, *94*, 201201.
[15] T. H. Liu, J. Zhou, B. Liao, D. J. Singh, G. Chen, *Phys. Rev. B* **2017**, *95*, 075206.
[16] J. Ma, A. S. Nissimagoudar, W. Li, *Phys. Rev. B* **2018**, *97*, 045201.
[17] J. Ma, Y. Chen, W. Li, *Phys. Rev. B* **2018**, *97*, 205207.
[18] S. Poncé, E. R. Margine, F. Giustino, *Phys. Rev. B* **2018**, *97*, 121201.
[19] T. H. Liu, B. Song, L. Meroueh, Z. Ding, Q. Song, J. Zhou, M. Li, G. Chen, *Phys. Rev. B* **2018**, *98*, 081203.
[20] F. Meng, J. Ma, J. He, W. Li, *Phys. Rev. B* **2019**, *99*, 045201.
[21] S. Poncé, D. Jena, F. Giustino, *Phys. Rev. B* **2019**, *100*, 085204.
[22] J. He, M. Amsler, Y. Xia, S. S. Naghavi, V. I. Hegde, S. Hao, S. Goedecker, V. Ozoliņš, C. Wolverton, *Phys. Rev. Lett.* **2016**, *117*, 046602.
[23] J. Park, Y. Xia, V. Ozoliņš, *Phys. Rev. Appl.* **2019**, *11*, 014058.
[24] P. Giannozzi, O. Andreussi, T. Brumme, O. Bunau, M. B. Nardelli, M. Calandra, R. Car, C. Cavazzoni, D. Ceresoli, M. Cococcioni, N. Colonna, I. Carnimeo, A. D. Corso, S. de Gironcoli, P. Delugas, R. A. DiStasio, A. Ferretti, A. Floris, G. Fratesi, G. Fugallo, R. Gebauer, U. Gerstmann, F. Giustino, T. Gorni, J. Jia, M. Kawamura, H. Y. Ko, A. Kokalj, E. Kçkbenli, M. Lazzeri, et al., *J. Phys.: Condens. Matter* **2017**, *29*, 465901.
[25] D. R. Hamann, *Phys. Rev. B* **2013**, *88*, 085117.
[26] P. Scherpelz, M. Govoni, I. Hamada, G. Galli, *J. Chem. Theory Comput.* **2016**, *12*, 3523.
[27] J. P. Perdew, K. Burke, M. Ernzerhof, *Phys. Rev. Lett.* **1996**, *77*, 3865.
[28] S. Poncé, E. Margine, C. Verdi, F. Giustino, *Comput. Phys. Commun.* **2016**, *209*, 116.
[29] S. Li, Z. Tong, H. Bao, *J. Appl. Phys.* **2019**, *126*, 025111.

[30] L. Zhang, P. Xiao, L. Shi, G. Henkelman, J. B. Goodenough, J. Zhou, *J. Appl. Phys.* **2015**, *117*, 155103.

[31] T. M. Tritt, M. A. Subramanian, *MRS Bull.* **2006**, *31*, 188.

[32] Y. Pei, H. Wang, G. J. Snyder, *Adv. Mater.* **2012**, *24*, 6125.

[33] A. Marini, C. Hogan, M. Grning, D. Varsano, *Comput. Phys. Commun.* **2009**, *180*, 1392.

[34] C. Verdi, F. Giustino, *Phys. Rev. Lett.* **2015**, *115*, 176401.

[35] T. Sohier, M. Gibertini, D. Campi, G. Pizzi, N. Marzari, *Nano Lett.* **2019**, *19*, 3723.

[36] B. Qiu, Z. Tian, A. Vallabhaneni, B. Liao, J. M. Mendoza, O. D. Restrepo, X. Ruan, G. Chen, *Europhys. Lett.* **2015**, *109*, 57006.

[37] T. H. Liu, J. Zhou, M. Li, Z. Ding, Q. Song, B. Liao, L. Fu, G. Chen, *Proc. Natl. Acad. Sci. USA* **2018**, *115*, 879.

[38] L. D. Zhao, S. H. Lo, Y. Zhang, H. Sun, G. Tan, C. Uher, C. Wolverton, V. P. Dravid, M. G. Kanatzidis, *Nature* **2014**, *508*, 373.

[39] L. D. Zhao, G. Tan, S. Hao, J. He, Y. Pei, H. Chi, H. Wang, S. Gong, H. Xu, V. P. Dravid, C. Uher, G. J. Snyder, C. Wolverton, M. G. Kanatzidis, *Science* **2016**, *351*, 141.

[40] C. Chang, M. Wu, D. He, Y. Pei, C. F. Wu, X. Wu, H. Yu, F. Zhu, K. Wang, Y. Chen, L. Huang, J. F. Li, J. He, L. D. Zhao, *Science* **2018**, *360*, 778.

[41] A. Dewandre, O. Hellman, S. Bhattacharya, A. H. Romero, G. K. H. Madsen, M. J. Verstraete, *Phys. Rev. Lett.* **2016**, *117*, 276601.

[42] B. Dongre, J. Carrete, S. Wen, J. Ma, W. Li, N. Mingo, G. K. H. Madsen, *J. Mater. Chem. A* **2020**, *8*, 1273.